NANO LETTERS

pubs.acs.org/NanoLett

Manipulating Quantum Dots to Nanometer Precision by Control of Flow

Chad Ropp,[†] Roland Probst,[‡] Zachary Cummins,[‡] Rakesh Kumar,[§] Andrew J. Berglund,[⊥] Srinivasa R. Raghavan,[§] Edo Waks,*[,†] and Benjamin Shapiro*[,∥]

[†]Department of Electrical and Computer Engineering, [‡]Department of Aerospace Engineering, [§]Department of Chemical and Biomolecular Engineering, and [∥]Fischell Department of Bio-Engineering, University of Maryland, College Park, Maryland 20742 and [⊥]Center for Nanoscale Science and Technology, National Institute of Standards and Technology, Gaithersburg, Maryland 20899

ABSTRACT We present a method for manipulating preselected quantum dots (QDs) with nanometer precision by flow control. The accuracy of this approach scales more favorably with particle size than optical trapping, enabling more precise positioning of nanoscopic particles. We demonstrate the ability to position a single QD in a 100 μm working region to 45 nm accuracy for holding times exceeding one hour and the ability to take active quantum measurements on the dynamically manipulated QD.

KEYWORDS Quantum dots, control, electroosmotic flow, subpixel averaging, photon antibunching

Manipulation and control of nanoscopic objects such as quantum dots (QDs) is a fundamental requirement for a broad range of applications in the fields of photonics, nanoelectronics, and biology. In particular, there is currently great interest in precise placement of preselected particles with desired properties, such as emission spectrum or brightness, on patterned or functionalized surfaces to engineer nanophotonic and nanoelectronic systems. Some important examples include the precise placement of single quantum dots in the high field region of both nanophotonic[1−3] and plasmonic[4,5] structures for scalable engineering of quantum information processors[6] and nanoscale electronic circuits.[7] Manipulation of QDs serving as biological tags could also enable in situ characterization of biological molecules and controlled investigation of biological processes.[8]

To date, the most notable successes of nanoparticle manipulation have been demonstrated using optical tweezers[9,10] and optofluidic devices.[11,12] These methods make movable active traps, either by laser-created optical gradient forces or by dynamic virtual electrodes that exert dielectrophoretic forces on polarizable particles. However, optical and dielectric forces scale with volume, making the trapping of nanoscopic objects such as QDs extremely challenging.[13] Furthermore, these trapping forces are nonspecific in that all particles are pulled in, resulting in a significant probability for capturing multiple objects. Multiparticle capture is a severe problem in quantum optics applications where the capture of multiple particles can ruin the single photon nature of the emission. In addition, for biological applications the use of high power lasers for optical trapping can easily damage biological objects.[14] Thus, development of particle manipulation methods that scale more favorably with particle size and do not require high-power lasers are needed.

Here we demonstrate a method to manipulate and position nanoscopic objects with nanometer precision in two dimensions without using traps. Instead, manipulation is achieved by moving the surrounding fluid via electroosmosis where an applied electric field moves a layer of surface ions that subsequently pulls the fluid, along with any suspended objects, by viscous drag.[15] The position of a chosen object is measured in real time with a microscope and a subpixel imaging algorithm that provides sub-wavelength-of-light precision.[16] Flow is then created to always move that object from its current location toward its desired position in discrete time steps, and it is this continual sensing and correction of errors (feedback control) that creates the nanometer precision. Since only the chosen object is always corrected back toward its target location, all other nearby objects are not controlled and drift away by a combination of random Brownian motion and diverging noncorrecting fluid flows at their locations in the device. This flow control approach is particularly promising for manipulation of extremely small dielectric particles, such as QDs, where trap-based approaches are limited[13] due to the small particle volumes. To demonstrate this advantage, this work focuses on the manipulation of single QDs which have an ellipsoidal core/shell structure and a radius of 6 nm (3 nm) on the major (minor) axis.

Flow control has previously been used to manipulate particles to micrometer precision.[17−23] Improved methods based on rotating laser sensing[24−27] enabled random capture of nanoscopic objects for short times with nanometer accuracy.[28−30] The ability to position and hold preselected

* Correspondence and request for materials should be addressed to E.W. (edowaks@umd.edu) or B.S. (benshap@umd.edu).

Received for review: 03/29/2010
Published on Web: 00/00/0000

DOI: 10.1021/nl101105j | *Nano Lett.* **XXXX,** *xxx,* 000–000

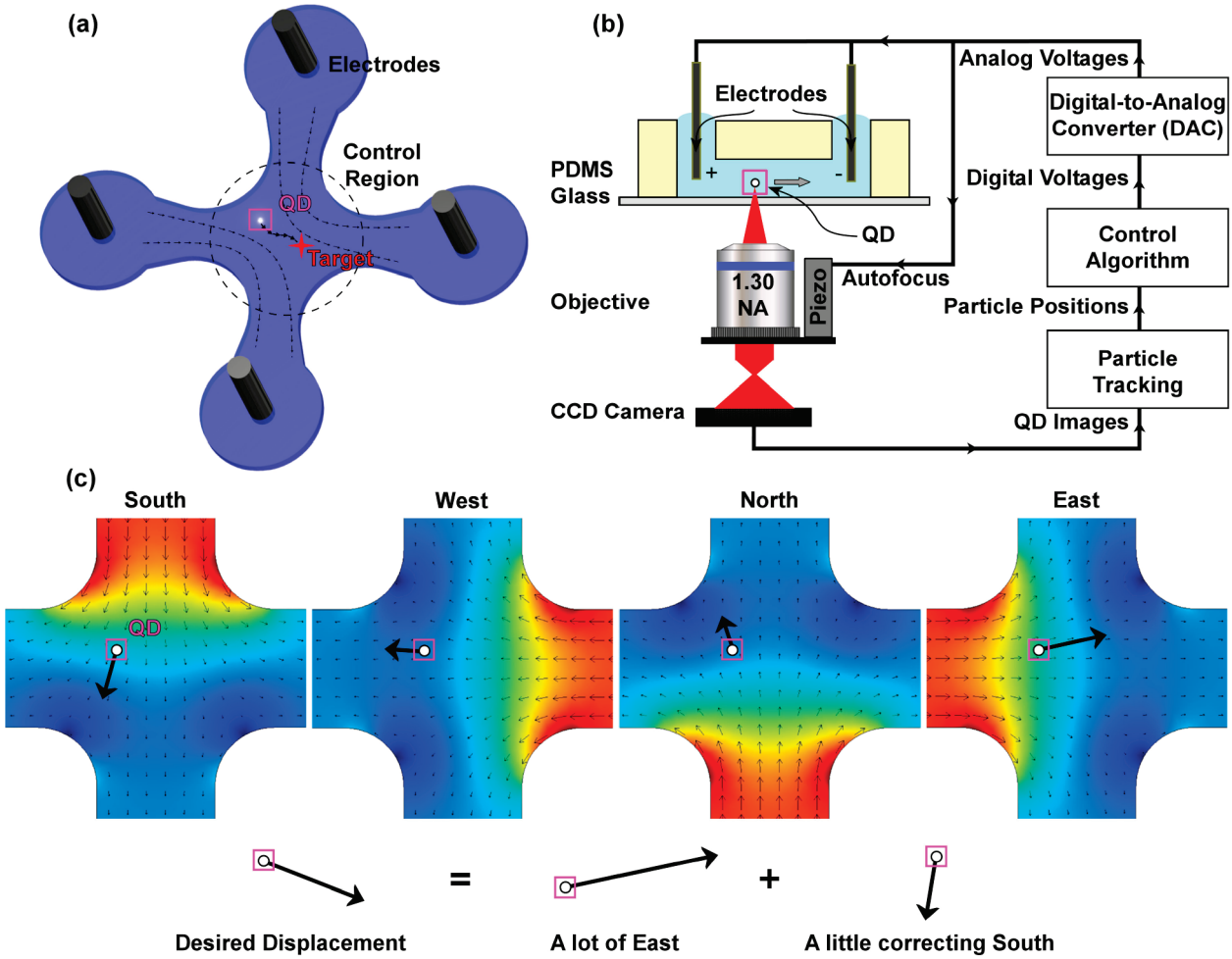

FIGURE 1. Experimental setup and control principle. (a) Schematic of our microfluidic device structure for 2D control of nanoparticles. An intersection between two microfluidic channels forms the control chamber of the device. Electrodes positioned in the fluid reservoirs actuate flow electroosmotically, while feedback is used to correctly move the nanoparticle to its target location. (b) Illustration of the optical and electronic setup for tracking and feedback control of QDs. A CCD camera images the QD and sends the information to a tracking algorithm that uses subpixel averaging to accurately determine the current position of the QD. The control algorithm uses this information to determine the proper voltage to apply to the electrodes in order to move the QD to its desired position. A second feedback loop moves the imaging objective in the *z*-direction using a piezo stage to keep the QD in focus. (c) Model of the four flow modes resulting from voltages applied to each electrode.[22,23] Any desired correcting velocity, at any particle location, can be created by combining these four actuation modes. (Black arrows show the microfluidic velocities, color shows the applied electric potential, and the enlarged black arrows show an example velocity decomposition.)

nanoscopic objects to nanometer precision has proven significantly more challenging due to their small size which both increases Brownian motion and makes it hard to accurately visualize their location. Quantum dots are particularly difficult to manipulate due to their inherent blinking which renders them optically invisible for prolonged periods of time.[31] During these "dark" periods, a QD can drift a significant distance away from its last observed location by diffusion. For this reason previous capturing methods were limited to 90 s trapping times.[21] The approach demonstrated here enables us to fully manipulate chosen nanoscopic objects in two dimensions. Any QD in the field of view can be moved from its current position to any desired location over a well-defined path with nanometer precision for times exceeding one hour. In addition, since we have the ability to manipulate the QD over a large control area, our technique is insensitive to QD blinking. When a QD blinks off, we can wait for it to blink back on and immediately reposition it back to the correct location even if it has drifted a significant distance away due to Brownian motion.

Figure 1a illustrates the device and operation principle used to manipulate single QDs using flow control. The device is composed of two microfluidic channels that intersect each other at a 90° angle. This design is first patterned into poly(dimethylsiloxane) (PDMS) and then adhered to a glass slide cover to form the microfluidic channels. The control region is located at the intersection of the two channels and is approximately 5 μm in height and 100 μm in diameter, though it can easily be made larger. Electroosmotic flow actuation is created by electrodes placed in four fluid reservoirs at the ends of the channels. The channels are subsequently filled with a water-based fluid containing CdSe/ZnS

DOI: 10.1021/nl101105j | *Nano Lett.* **XXXX,** *xxx,* 000–000

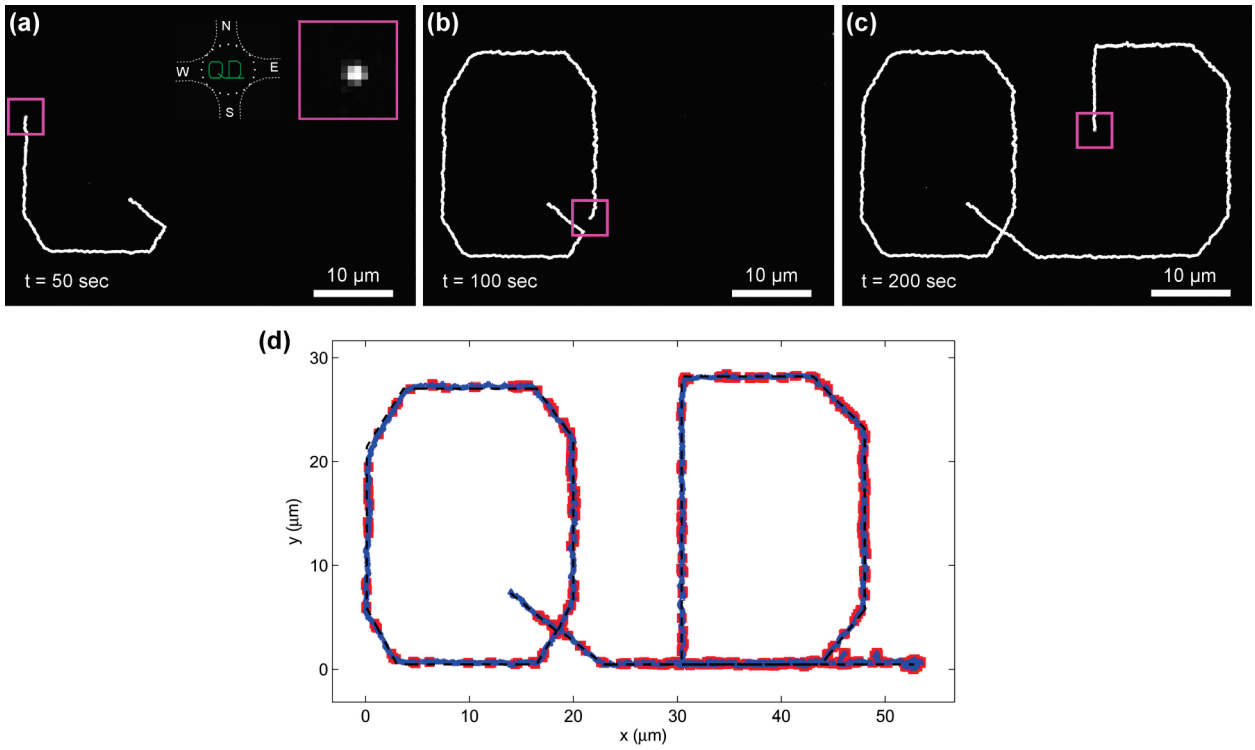

FIGURE 2. Single quantum dot trajectory. (a–c) Time-stamped CCD camera images of a single quantum dot being steered along the desired trajectory (the movie is provided in the Supporting Information). The white trace shows the measured path of the quantum dot up until its current location. The square magenta box shows the subpixel averaging window used to determine the current position of the QD. The insets in panel a show the orientation of the channel with the trajectory (green) and a close-up of the subpixel averaging window which contains the QD near its center. (d) Plot of quantum dot position along its trajectory. The dotted black line shows the desired trajectory programmed into the controller. The actual measured QD trajectory is shown in blue. The solid red squares depict when the quantum dot blinks off. At the end of the trajectory the QD is held in place for 2 min. The mean displacement from the trajectory is calculated to be 119.5 nm.

QDs (Qdot 655 nm ITK amino), along with a mixture of mass fraction 1.25% of an associating polymer (RM-825, Rohm and Haas Co.)[32] and 0.55% of a zwitterionic betaine surfactant.[33] The associating polymer is used to increase the viscosity of the fluid to 0.23 Pa s by hydrophobic clustering[32] in order to decrease QD Brownian motion, while the surfactant is used to enhance fluid actuation. The colloidal QDs are illuminated with 532 nm light at an intensity of 250 W/cm^2 and imaged using an inverted confocal microscope.

The entire tracking system with the feedback control loop is depicted in Figure 1b. Images are acquired from a CCD camera at a 20 Hz frame rate and then processed in real time using a centroid algorithm to precisely determine the position of the QD. The control algorithm then calculates the voltages needed to move that QD to its desired location by decomposing the needed correction vector into the components that can be actuated by each pair of electrodes, as illustrated in Figure 1c, and by determining the ratio of the voltage differences that will create this desired direction. The magnitude of the actuation is then set by a control gain. In our device, the size of the electroosmotic actuation can depend somewhat on the height of the QD due to a different zeta potential at the top PDMS versus the bottom glass substrate. Electrophoretic forces can also contribute to the actuation, but for QDs they are much weaker than the actuation due to electroosmotic flow. The control gain is set to an intermediate value that achieves good manipulation over the entire height of the device. Once computed, the necessary voltages are then applied to each of the four electrodes to move the QD as desired. Platinum electrodes are used to minimize unwanted electrochemistry effects in the fluid.[15] Although the target QD is controlled in the plane, the QD can still drift slowly in the third dimension causing it to go out of focus and thus degrade the performance of the vision-based control. To correct this, the imaging objective is mounted on a piezo stage and a second Newton-bracketing feedback control algorithm uses the width of the QD image as its metric to track the QD in the z direction, thus keeping it in focus. This improves control precision in the xy plane.

The ability to accurately manipulate QDs in two dimensions is shown in Figure 2. A single QD is selected from the 100 μm × 100 μm control region which contains approximately 10 QDs. A small area around the QD, denoted by the box, defines the 16 pixel ×16 pixel tracking window used to calculate the QD position via the centroid algorithm. Panels a–c show the position of a single QD at several different times as it is controlled along a well-defined path (the movie is provided in the Supporting Information). The inset to Figure 2a shows the orientation of the trajectory with

DOI: 10.1021/nl101105j | *Nano Lett.* **XXXX,** *xxx,* 000–000

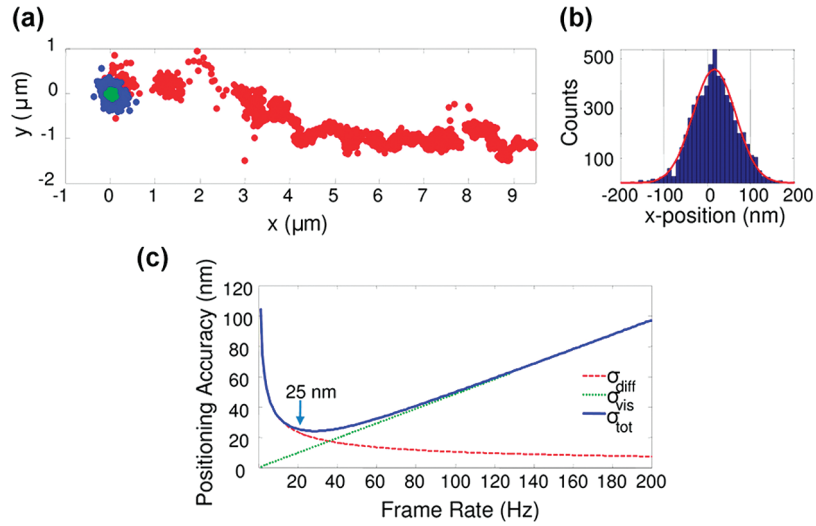

FIGURE 3. QD positioning accuracy. (a) Blue points represent the measured position of the QD as it is held in place for 5 min. The standard deviation along x of the blue points is calculated to be 49.3 nm. The controller is subsequently turned off, and the QD is allowed to drift away for another 5 min, as shown by the red points. The drift to the east is caused by a small pressure flow in the device, a flow that is continuously corrected for when feedback control is on. Measured positions of a QD adhered to glass are shown in green. This corresponds to the vision accuracy of the setup and has a standard deviation along x of 18.8 nm. Subtracting the vision noise from our measured variance demonstrates that we are positioning with 45.5 nm accuracy. (b) Positions along the x direction of the held QD with a Gaussian fit using $\sigma = 49.3$ nm. The center of the Gaussian is slightly to the right of zero corresponding to the small pressure flow toward the east. (c) Calculated positioning accuracy due to diffusion (dashed red line), vision noise (dotted green line), and both noise sources combined (solid blue line) as a function of camera frame rate.

respect to the cross channel and a close-up of the tracking window. The desired position was progressed along the fixed trajectory at a speed of 2 μm/s while the control algorithm continuously adjusted the applied voltages to move the QD toward this moving target. In order to determine whether the QD had blinked off, a threshold camera intensity was selected. When the camera signal fell below this threshold, all voltages were switched to zero and the controller halted to wait for the QD to begin re-emitting. During the wait for the QD to resume photon emission, the tracking region was temporarily expanded to three times its size to ensure that Brownian motion would not carry the QD out of the detection window before it began re-emitting. The full trace of the QD position is shown in Figure 2d and is overlaid on the desired trajectory. The times when the QD blinks "off" are shown in red. Analysis of the position data found that the average displacement of the QD from the path was 119.5 nm.

To determine the positioning precision of the control method, a single QD was selected and moved to a specified location near the center of the control region. The QD was held in that position by feedback control and monitored for a 5 min time span, after which the control was turned off and the QD was allowed to freely diffuse for another 5 min. Figure 3a shows the measured positions of the trapped (blue spots) and freely diffusing (red spots) QD. The accuracy of the centroid algorithm in detecting the particle location was determined independently by taking position measurements on a QD that was adhered on a glass slide and was therefore immobile, for 5 min. The measured positions of the adhered QD are plotted in Figure 3a as green spots. From the variance of the green spots we determined the vision noise to be 18.8 $\pm$ 0.9 nm (18.7 $\pm$ 1.7 nm) in the x (y) direction. Figure 3b plots a histogram of the x-positions of the held QD, and from the Gaussian fit the standard deviation was found to be 49.3 $\pm$ 0.7 nm. A similar calculation gives a standard deviation 47.0 $\pm$ 0.7 nm in the y positions. The measured fluctuation in QD position is due to a combination of the random motion of the particle and vision noise of the imaging. Subtracting the measured vision noise, we determine the actual positioning precision of the particle to be 45.5 $\pm$ 0.9 nm (43.1 $\pm$ 1.0 nm) in the x (y) direction.

The achieved precision is enabled by feedback, the continual sensing and correction of the QD's deviation from its desired location, and it is successful even if the flow fields in the device are not known perfectly. So long as the actuation is sufficient to move the QD from where it is *toward* where it should be, the control acts to significantly decrease the position error at each time, quickly driving the QD to its desired location. The resulting positioning accuracy of the control is fundamentally limited by the Brownian motion of the particle between control updates and the accuracy of the vision sensing[27] and is thus given by $\sigma^2_{\text{total}} = \sigma^2_{\text{diff}} + \sigma^2_{\text{vision}}$. In this expression, $\sigma^2_{\text{diff}} = 2D/F$ is the noise due to diffusion where D is the diffusion coefficient and F is the camera frame rate. For a spherical particle of radius a in the limit of low Reynold's number, the diffusion coefficient is given by the Einstein–Stokes relation $D = k_B T/(6\pi\eta a)$ where k_B is the Boltzmann constant, T is the fluid temperature, and η is the fluid viscosity. The second noise term σ^2_{vision} is the camera vision noise which is primarily due to photon shot noise and camera read noise (background noise was deter-

DOI: 10.1021/nl101105j | *Nano Lett.* **XXXX,** *xxx,* 000–000

mined to be negligibly small compared to these noise sources) and is given by

$$\sigma^2_{\text{vision}} = \frac{\lambda^2 F}{8R} + \frac{d^2_{\text{pix}} n_r^2 \sigma_u^2 F^2}{R^2}$$

The first term in the above expression accounts for shot noise, while the second term accounts for read noise which is assumed to be equal for each pixel. The parameter λ is the emission wavelength of the QD, R is the total photon detection rate integrated over the entire camera image, n_r is the camera read noise, d_{pix} is the distance on the sample represented by the separation between adjacent pixels, and $\sigma_u^2 = N^2(N/2 + 1)(N + 1)/6$ where N is the size of the subpixel averaging window. We note that out of all the noise sources, only σ^2_{diff} depends on the size of the particle, and this dependence occurs through the diffusion coefficient which is inversely proportional to the particle radius. Thus, the positioning precision scales inversely with particle radius, in contrast to optical traps where it scales inversely with radius cubed.[9]

To determine the theoretical positioning limit, the camera read noise was measured to be 6.3 electrons, d_{pix} was measured to be 160 nm, and the peak photon detection rate was determined from the CCD image intensity to be $R = 175000\ \text{s}^{-1}$. It should be noted that the photon detection rate varied significantly throughout this experiment due to blinking and intensity noise of the QD emitter. The diffusion coefficient was directly measured to be $(5.5 \pm 0.4) \times 10^{-15}$ m^2/s by tracking free floating QDs in the microfluidic chamber and performing a maximum likelihood estimate on the data. This measured diffusion coefficient differs significantly from the number that would be calculated by the Stokes–Einstein relation using the particle radius and measured viscosity. This discrepancy is well-known and is attributed to the fact that the particle interacts with the nearby liquid to create an effective *hydrodynamic diameter* that can be much larger than the actual diameter of the particle.[34] We thus use the measured diffusion coefficient in our calculations.

Setting the QD emission wavelength to λ=655 nm, we plot σ_{diff}, σ_{vision}, and σ_{total} as a function of the camera frame rate in Figure 3c. From the plot one can see that there is a trade-off between vision noise and Brownian motion. As the frame rate is increased, noise due to Brownian motion is reduced because the particle has had less time to diffuse between successive camera frames but vision noise increases because fewer photons are collected from the QD. At 20 Hz the limit to the position accuracy is given by 25 nm. The optimal position accuracy of 24 nm is achieved at a frame rate of 28 Hz, which is very close to the actual frame rate our system is operating at. The experimental results do not achieve the theoretical positioning limit due to additional noise sources such as mechanical vibration and instability, imperfections in the control algorithms, and frame averaging effects caused by the fact that the QD is moving during the acquisition of a single camera image.

To investigate the trapping time, we positioned and trapped a second QD for 1 h. From the position data it was found that this QD was held with 51.5 ± 0.8 nm precision. The slight increase in position error was due to the fact that by the end of the 1 h, the QD was emitting much less brightly and blinking significantly more due to oxygen contamination and photobleaching. The increase in blinking served to reduce the position precision because the QD was able to drift for a longer distance before re-emitting. This degradation is attributed to oxygen contamination and be can be reduced by incorporating oxygen scavenging chemicals in the solution.[35] At no time during the 1 h period were multiple QDs inadvertently trapped by the controller. To our knowledge, such trapping times for single QDs have not been demonstrated using other fluidic trapping methods. For comparison, the nonspecific trap created by an optical tweezer will typically trap additional quantum dots on a time scale of 5–10 min.[10]

To ensure that we are controlling a single QD and to demonstrate that we can characterize the single photon nature of our emitter while simultaneously performing control, we carried out an autocorrelation on a dynamically positioned QD. A 25–75 beam splitter was used to deflect 75% of the light away from the camera and into a Hanbury–Brown–Twiss (HBT) type autocorrelation measurement composed of a 50–50 beamsplitter and two avalanche photodiodes. The remaining 25% was sent onto the CCD camera to position the QD at a fixed location in the microfluidic device. To reduce uncorrelated background counts, we gated the autocorrelation setup to accumulate data only when the QD was not blinked off using the intensity threshold from the CCD camera image. The results of the autocorrelation measurement which was taken over 15 min are shown in Figure 4. The autocorrelation was fit to a function of the form $G^2(\tau) = G^2_\infty[1 - (1 - g^2(0))e^{-\Gamma\tau}]$, where $\Gamma = \Gamma_s + \Gamma_e$ with Γ_s being the spontaneous emission rate and Γ_e being the excitation rate. In our experiment the excitation power was set to 250 W/cm^2, which is well below saturation.[36,37] In this limit the excitation rate is much smaller that the spontaneous emission rate so $\Gamma \approx t_s^{-1}$ where t_s is the QD spontaneous emission lifetime. From the data fit we find that $g^2(0) = 0.37 \pm 0.02$, which is a clear signature of antibunching demonstrating that we are indeed controlling a single QD. The fit also yields a QD spontaneous emission time of $t_s = 22.7 \pm 1.1$ ns, which is consistent with previously measured values.[36,37,28] This result ensures that we can use the QD as a single photon source for integration with nanophotonic structures while simultaneously positioning it with flow control.

In conclusion, we have shown the ability to individually select, characterize, and position single nanoscopic objects with nanometer precision. In our current experiments,

DOI: 10.1021/nl101105j | *Nano Lett.* **XXXX,** *xxx,* 000–000

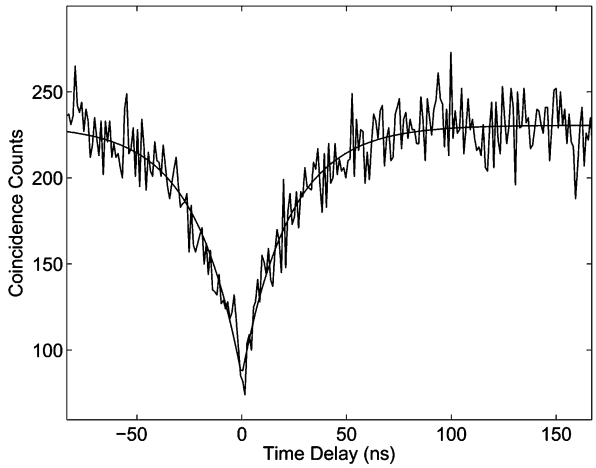

FIGURE 4. In situ autocorrelation measurement of a single QD. Autocorrelation measurement of a single controlled quantum dot obtained from a 15 min integration with 1 ns binning and with exponential fits shown. From the exponential fit, we determine $g^2(0) = 0.37 \pm 0.02$ and decay time $t_d = 22.7 \pm 1.1$ ns.

control can only be achieved in two dimensions for individual quantum dots. However, recent theoretical work has shown that it is possible to achieve three-dimensional control in novel two-layer microfluidic devices.[38] It is also possible to extend the control to multiple particles using techniques experimentally demonstrated in ref 23. Our capabilities could enable integration of single quantum dots, or other visualizable nanoscale objects, with photonic structures and enable the development of novel nanophotonic devices and sensors. Additional techniques providing immobilization of objects via surface chemistry[39] or cross-linking polymerization[40] could be further incorporated with the procedure demonstrated here for scalable fabrication of integrated devices that require the precise placement of preselected nanoparticles with desired properties.

Acknowledgment. We thank Sina Sahand for help with device design and Kunshan Sun for his help with viscosity and diffusion measurements. This work was supported by a DARPA Defense Science Office seed grant (Grant Number W31P4Q0810007). Dr. Shapiro also acknowledges funding support from the National Science Foundation CAREER award (Grant Number ECS0348251). Certain commercial equipment, instruments, or materials are identified in this paper to foster understanding. Such identification does not imply recommendation or endorsement by the National Institute of Standards and Technology, nor does it imply that the materials or equipment identified are necessarily the best available for the purpose.

Supporting Information Available. A movie showing the dynamic positioning of a single quantum dot corresponding to Figure 2. In the movie the tracking cursor becomes a triangle and the electrode voltages (bottom left) are set to zero when the quantum dot blinks "off." This material is available free of charge via the Internet at http://pubs.acs.org.

REFERENCES AND NOTES

(1) Badolato, A.; Hennessy, K.; Atature, M.; Dreiser, J.; Hu, E.; Petroff, P. M.; Imamoglu, A. *Science* **2005**, *308*, 1158–1161.
(2) Hennessy, K.; Badolato, A.; Winger, M.; Gerace, D.; Atature, M.; Gulde, S.; Falt, S.; Hu, E. L.; Imamoglu, A. *Nature* **2007**, *445*, 896–899.
(3) Englund, D.; Faraon, A.; Fushman, I.; Stoltz, N.; Petroff, P.; Vuckovic, J. *Nature* **2007**, *450*, 857–861.
(4) Akimov, A. V.; Mukherjee, A.; Yu, C. L.; Chang, D. E.; Zibrov, A. S.; Hemmer, P. R.; Park, H.; Lukin, M. D. *Nature* **2007**, *450*, 402–406.
(5) Schietinger, S.; Barth, M.; Aichele, T.; Benson, O. *Nano Lett.* **2009**, *9*, 1694–1698.
(6) Waks, E.; Vuckovic, J. *Phys. Rev. Lett.* **2006**, *96*, 153601–4.
(7) Engheta, N. *Science* **2007**, *317*, 1698–1702.
(8) Medintz, I. L.; Uyeda, H. T.; Goldman, E. R.; Mattoussi, H. *Nat. Mater.* **2005**, *4*, 435–446.
(9) Ashkin, A.; Dziedzic, J. M.; Bjorkholm, J. E.; Chu, S. *Opt. Lett.* **1986**, *11*, 288–290.
(10) Jauffred, L.; Richardson, A. C.; Oddershede, L. B. *Nano Lett.* **2008**, *8*, 3376–3380.
(11) Chiou, Pei-Yu; Ohta, A.; Jamshidi, A.; Hsu, Hsin-Yi; Wu, M. *J. Microelectromech. Syst.* **2008**, *17*, 525–531.
(12) Yang, A. H. J.; Moore, S. D.; Schmidt, B. S.; Klug, M.; Lipson, M.; Erickson, D. *Nature* **2009**, *457*, 71–75.
(13) Dienerowitz, M.; Mazilu, M.; Dholakia, K. *J. Nanophotonics* **2008**, *2*, No. 021875.
(14) Neuman, K.; Chadd, E.; Liou, G.; Block, S. *Biophys. J.* **1999**, *77*, 2856–2863.
(15) Probstein, R. F. *Physicochemical hydrodynamics*; John Wiley and Sons: New York, 1994.
(16) Thompson, R. E.; Larson, D. R.; Webb, W. W. *Biophys. J.* **2002**, *82*, 2775–2783.
(17) Armani, M.; Chaudhary, S.; Probst, R.; Shapiro, B. uTAS 2004, Malmo, Sweden 2004.
(18) Armani, M.; Chaudhary, S.; Probst, R.; Shapiro, B. *IEEE Int. Conf. Micro Electro Mechan. Syst., Miami, FL, 18th* **2005**, 855–858.
(19) Cohen, A. E.; Moerner, W. E. *Appl. Phys. Lett.* **2005**, *86*, 093109–3.
(20) Cohen, A. E. *Phys. Rev. Lett.* **2005**, *94*, 118102.
(21) Cohen, A. E.; Moerner, W. E. *Proc. Natl. Acad. Sci. U.S.A.* **2006**, *103*, 4362–4365.
(22) Chaudhary, S.; Shapiro, B. *IEEE Trans. Contr. Syst. Technol.* **2006**, *14*, 669–680.
(23) Armani, M.; Chaudhary, S.; Probst, R.; Shapiro, B. *J. Microelectromech. Syst.* **2006**, *15*, 945–956.
(24) Enderlein, J. *Appl. Phys., B: Lasers Opt.* **2000**, *71*, 773–777.
(25) Levi, V.; Ruan, Q.; Kis-Petikova, K.; Gratton, E. *Biochem. Soc. Trans.* **2003**, *31*, 997–1000.
(26) Berglund, A.; Mabuchi, H. *Opt. Express* **2005**, *13*, 8069–8082.
(27) Berglund, A.; Mabuchi, H. *Appl. Phys., B: Lasers Opt.* **2006**, *83*, 127–133.
(28) McHale, K.; Berglund, A. J.; Mabuchi, H. *Nano Lett.* **2007**, *7*, 3535–3539.
(29) Cohen, A. E.; Moerner, W. E. *Opt. Express* **2008**, *16*, 6941–6956.
(30) Jiang, Y.; Wang, Q.; Cohen, A. E.; Douglas, N.; Frydman, J.; Moerner, W. E. In *Optical Trapping and Optical Micromanipulation V*; SPIE: San Diego, CA, 2008; Vol. 7038, pp 703807-12.
(31) van Sark, W. G. J. H. M.; Frederix, P.; Bol, A. A.; Gerritsen, H. C.; Meijerink, A. *ChemPhysChem* **2002**, *3*, 871–879.
(32) Kumar, R.; Raghavan, S. R. *Langmuir* **2010**, *26*, 56–62.
(33) Kumar, R.; Kalur, G. C.; Ziserman, L.; Danino, D.; Raghavan, S. R. *Langmuir* **2007**, *23*, 12849–12856.
(34) Borsali, R.; Pecora, R. *Soft Matter*, **2008**.
(35) Hohng, S.; Ha, T. *J. Am. Chem. Soc.* **2004**, *126*, 1324–1325.
(36) Michler, P.; Imamoglu, A.; Mason, M. D.; Carson, P. J.; Strouse, G. F.; Buratto, S. K. *Nature* **2000**, *406*, 968–970.
(37) Lounis, B.; Bechtel, H. A.; Gerion, D.; Alivisatos, P.; Moerner, W. E. *Chem. Phys. Lett.* **2000**, *329*, 399–404.
(38) Probst, R.; Shapiro, B. *Lab Chip* Submitted.
(39) Zhang, Q.; Dang, C.; Urabe, H.; Wang, J.; Sun, S.; Nurmikko, A. *Opt. Express* **2008**, *16*, 19599–19592.
(40) Liu, J.; Gao, D.; Li, H.; Lin, J. *Lab Chip* **2009**, *9*, 1301–1305.

DOI: 10.1021/nl101105j | *Nano Lett.* **XXXX,** *xxx,* 000–000